VOLUME 118, NUMBER 6
FEBRUARY 14, 1996

JOURNAL OF THE AMERICAN CHEMICAL SOCIETY

Electronically Excited States of 1,4:5,8-Bismethano-1,4,4a,5,8,8a-hexahydronaphthalene, a Nonconjugated Diene: Comparison of Theory and Experiment

Daniel E. Love,[†] Dana Nachtigallova,[†] Kenneth D. Jordan,*[,†] James M. Lawson,[‡] and Michael N. Paddon-Row[‡]

Contribution from the Department of Chemistry, University of Pittsburgh, Pittsburgh, Pennsylvania 15260, and School of Chemistry, University of New South Wales, Sydney 2052, Australia

Received October 16, 1995[⊗]

Abstract: Electron energy-loss spectroscopy (EELS) is used to determine the energies of low-lying singlet and triplet states of the title compound. The EELS measurements give a splitting of 0.45 eV between the two lowest $\pi \rightarrow \pi^*$ singlet states, as confirmed by optical absorption measurements, but do not give a discernable splitting between the corresponding triplet states. The experimental results are interpreted with the aid of ab initio electronic structure calculations using the CIS and CASPT2 methods. The calculations are consistent with the experiments, giving a much larger splitting between the $\pi \rightarrow \pi^*$ singlet as compared to the $\pi \rightarrow \pi^*$ triplet states. They also reveal that the splitting between the two lowest $\pi \rightarrow \pi^*$ triplet states is dominated by through-bond (TB) interactions, whereas that between the corresponding singlet states includes also a significant contribution from the dipole−dipole coupling mechanism.

1. Introduction

The nonconjugated diene 1,4:5,8-bismethano-1,4,4a,5,8,8a-hexahydronaphthalene (**1**) has played a pivotal role in the evolution of our understanding of through-bond coupling[1] in molecules. At the geometry of the ground state of the neutral molecule the π cation and π^* anion states of **1** are split by 0.87 and 0.80 eV, respectively.[2,3] Theoretical studies[4−7] have shown

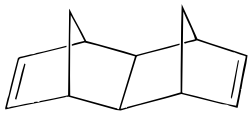

1

that these splittings are about an order of magnitude greater than would exist were only direct through-space interactions operative between the ethylenic groups. In fact, the splittings are mainly due to through-bond coupling[1] brought about by mixing of the localized ethylenic π and π^* orbitals with the σ and σ^* orbitals of the bridge. Although the cation and anion states of **1** have been extensively studied both experimentally[2,3] and theoretically,[4−7] no work has been done on the electronically excited states of this molecule.

In the present study, electron energy-loss spectroscopy is used to characterize the low-lying singlet and triplet states of **1** in the gas phase and to determine whether core-excited anion states significantly enhance the cross section for formation of the π

[†] University of Pittsburgh.
[‡] University of New South Wales.
[⊗] Abstract published in *Advance ACS Abstracts,* February 1, 1996.

(1) Hoffmann, R. *Acc. Chem. Res* **1971**, *4*, 1. Hoffmann, R.; Imamura, A.; Hehre, W. J. *J. Am. Chem. Soc.* **1968**, *90*, 1499.
(2) Paddon-Row, M. N.; Patney, J. K.; Brown, R. S.; Houk, K. N. *J. Am. Chem. Soc.* **1981**, *103*, 5575.
(3) Balaji, V.; Jordan, K. D.; Burrow, P. D.; Paddon-Row, M. N.; Patney, J. K. *J. Am. Chem. Soc.* **1982**, *104*, 6849.
(4) Jordan, K. D.; Paddon-Row, M. N. *Chem. Rev.* **1992**, *92*, 395.
(5) Paddon-Row, M. N.; Wong, S. S. *Chem. Phys. Lett.* **1990**, *167*, 432.
(6) Jordan, K. D.; Paddon-Row, M. N. *J. Phys. Chem.* **1992**, *96*, 1188.
(7) Kim, K.; Jordan, K. D.; Paddon-Row, M. N. *J. Phys. Chem.* **1994**, *98*, 10089.

0002-7863/96/1518-1235$12.00/0

$\rightarrow \pi^*$ excited states. In addition, the optical absorption spectrum of **1** in acetonitrile is measured for wavelengths between 185 and 400 nm. To aid in the interpretation of the experimental spectrum the excitation energies of **1** are calculated by means of the single excitation CI (CIS),[8] complete-active-space self-consistent-field (CASSCF), and complete-active-space multi-reference second-order perturbation (CASPT2) theoretical methods.[9]

2. Methodology

(1) Experimental Methods. The electron energy-loss spectrometer (EELS) used in this study has been described elsewhere,[10,11] and only a brief description is given here. The EELS system consists of a single-stage trochoidal analyzer[12] to select the energy of the incident electrons, which are passed through a static cell where scattering with the target gas takes place, a dual-stage trochoidal analyzer to analyze the residual energy of the scattered electrons, and a dual microchannel plate detector. Most of the spectra are obtained in the fixed residual energy (E_{res}) mode of operation of the spectrometer, where $E_{res} = E_{inc} - E_{loss}$. The spectrometer was tuned so that the overall resolution was about 80 meV.

(2) Theoretical Methods. With the molecular orientation used in this study, the bonding (π_+) and antibonding (π_-) combinations of the ethylenic π orbitals of **1** are of a_1 and b_2 symmetry, respectively, and the bonding (π^*_+) and antibonding (π^*_-) combinations of the ethylenic π^* orbitals are of b_1 and a_2 symmetry, respectively. The $\pi_+(a_1) \rightarrow \pi^*_+(b_1)$ and $\pi_-(b_2) \rightarrow \pi^*(a_2)$ transitions are of B_1 symmetry, and the $\pi_+(a_1) \rightarrow \pi^*(a_2)$ and $\pi_-(b_2) \rightarrow \pi^*_+(b_1)$ transitions are of A_2 symmetry. The two configurations of each symmetry mix, making single-configurational methods unsuitable for describing the $\pi \rightarrow \pi^*$ excited states.

In both the triplet and singlet manifolds, the $\pi \rightarrow \pi^*$ states "separate" into two lower energy "local" states (one each of B_1 and A_2 symmetry) and two higher lying "charge-transfer" states (again, one each of B_1 and A_2 symmetry). In terms of localized orbitals, the charge-transfer states are dominated by the $\pi_L^2\pi_L^*\pi_R$ and $\pi_L\pi_R^2\pi_R^*$ configurations, and the local states are dominated by the $\pi_L\pi_L^*\pi_R^2$ and $\pi_L^2\pi_R\pi_R^*$ configurations, where "L" and "R" designate orbitals localized on one or the other ethylenic groups. The splittings between the local $\pi \rightarrow \pi^*$ states of B_1 and A_2 symmetry provide a measure of the electronic couplings in the triplet and singlet manifolds. In the case of the triplet states, both through-space and through-bond interactions contribute to the splitting, with the latter expected to be dominant. In the singlet manifold, the dipole−dipole (Forster) coupling mechanism[13] is also operative. As a result, the splitting between the two lowest singlet $\pi \rightarrow \pi^*$ states is expected to be larger than that between the corresponding triplet states.

For norbornadiene it has been found that the second and higher lying $\pi \rightarrow \pi^*$ singlet transitions are overlapped with Rydberg states.[10,14] This is also likely to be the case for **1**, making it necessary to employ in the theoretical calculations basis sets sufficiently flexible to describe both the valence and low-lying Rydberg states.[15]

In the CIS method[8] the excited states are described as linear combinations of configurations that are singly excited with respect to the Hartree−Fock wave function for the ground electronic state. The CIS method allows for orbital relaxation and accounts for near degeneracy effects, such as the mixing between the $\pi \rightarrow \pi^*$ configurations of the same symmetry. However, it does not describe dynamical correlation effects, and thus may not correctly order valence and Rydberg states. The CIS calculations were carried out using the Gaussian 92 program.[16]

The more computationally demanding CASPT2 method allows also for dynamical correlation effects, and has been found to provide an accurate description of $\pi \rightarrow \pi^*$ excited states of ethylene and other, more complex, molecules.[15] In this method, CASSCF calculations are carried out for each state of interest and the resulting CASSCF wave functions and orbitals are used to carry out multi-reference MP2 calculations. The CASSCF and CASPT2 calculations were performed using the MOLCAS3 program.[17]

The ANO' basis set used for the CASPT2 calculations was formed by adding diffuse primitive s, p, and d functions to the contracted (3s3p1d/3s2p/2s) ANO Gaussian basis set.[18] The (3s3p1d/3s2p/2s) designation indicates that the (3s3p1d) and (3s2p) ANO basis sets were employed on the ethylenic and non-ethylenic C atoms, respectively, and that the (2s) ANO basis set was used on the H atoms. The diffuse functions were located at the center of charge of the ground state radical cation of **1**, and their exponents were optimized for the 3s, 3p, and 3d Rydberg orbitals obtained from Hartree−Fock calculations on the cation. The CIS calculations were performed using the 6-31G basis set,[19] augmented with d polarization functions and diffuse sp ("+") functions[20] on the ethylenic carbon atoms, and with the same Rydberg orbitals as used in the ANO' basis set. CIS and CASPT2 calculations were also carried out using the 3-21G basis set.[21] The 3-21G basis set does not have the flexibility needed for obtaining accurate excitation energies, and is included only to determine whether such a modest-sized basis set is able to describe the splittings between the $\pi \rightarrow \pi^*$ singlet and triplet states. Unless noted otherwise, the discussion will focus on the results obtained with the basis sets that include the diffuse functions.

The active spaces for the CASPT2 calculations with the ANO' basis set included the a_1 and b_2 π and the b_1 and a_2 π^* valence orbitals, as well as subsets of the 3s, 3p, and 3d Rydberg orbitals. Specifically, the active space used for the excited states of B_1 and A_2 symmetry included the 3p and 3d Rydberg orbitals of b_1 and a_2 symmetry, and that used for the A_1 and B_2 Rydberg states included the 3s, 3p, and 3d Rydberg orbitals of a_1 and b_2 symmetry. In order to minimize the effect of intruder states, extra virtual orbitals (one each of b_1 and a_2 symmetry in the calculations of the B_1 and A_2 states, and one each of a_1 and b_2 symmetry in the calculations of the A_1 and B_2 states) were included in the active spaces. Together these two active spaces permit a description, in both the singlet and triplet manifolds, of the two B_1 and two A_2 $\pi \rightarrow \pi^*$ valence states as well as the six A_1, six B_2, three B_1, and three A_2 Rydberg states derived from the $\pi \rightarrow$ 3s, $\pi \rightarrow$ 3p, and $\pi \rightarrow$ 3d excitations. In addition, as a result of the inclusion of the extra virtual orbitals to avoid problems associated with intruder states, the active spaces also describe a subset of the possible $\pi \rightarrow \sigma^*$ states. For each of the two active spaces, CASPT2 calculations were also performed for the ground electronic state, and the resulting ground state energies were subtracted from the excited state energies in order to obtain excitation energies.

Convergence problems were encountered when performing CASSCF

(8) Foresman, J. B.; Head-Gordon, M.; Pople, J. A.; Frisch, M. J. *J. Phys. Chem.* **1992**, *96*, 135.
(9) Anderson, K.; Malmqvist, P.-A.; Roos, B. O.; Sadlej, A. J.; Wolinski, K. *J. Chem. Phys.* **1990**, *94*, 5483. Anderson, K.; Malmqvist, P.-A.; Roos, B. O. *J. Chem. Phys.* **1992**, *96*, 1218.
(10) Allan, M. *J. Electron Spectrosc. Relat. Phenom.* **1989**, *48*, 219.
(11) Falcetta, M. F.; Jordan, K. D. *J. Am. Chem. Soc.* **1991**, *113*, 7455.
(12) Stamatovic, A.; Schulz, G. J. *Rev. Sci. Instrum.* **1970**, *41*, 423.
(13) Forster, Th. *Discuss. Faraday Soc.* **1959**, *27*, 7.
(14) Roos, B. O.; Merchan, M.; McDiarmid, R.; Xing, X. *J. Am. Chem. Soc.* **1994**, *116*, 5927.
(15) Roos, B. O.; Serrano-Andres, L.; Merchan, M. *Pure Appl. Chem.* **1993**, *65*, 1693. Serrano-Andres, L.; Merchan, M.; Nebot-Gil, I.; Roos, B. O.; Fulscher, M. P. *J. Am. Chem. Soc.* **1993**, *115*, 6184. Serrano-Andres, L.; Merchan, M.; Nebot-Gil, I.; Lindh, R.; Roos, B. O. *J. Chem. Phys.* **1993**, *98*, 3151. Serrano-Andres, L.; Roos, B. O.; Merchan, M. *Theor. Chim. Acta* **1994**, *87*, 387. Rubio, M.; Merchan, M.; Orti, E.; Roos, B. O. *Chem. Phys.* **1994**, *179*, 395.
(16) Frisch, M. J.; Trucks, G. W.; Schlegel, H. B.; Gill, P. M. W.; Johnson, B. G.; Wong, M. W.; Foresman, J. B.; Robb, M. A.; Head-Gordon, M.; Replogle, E. S.; Gomperts, R.; Andres, J. L.; Raghavachari, K.; Binkley, J. S.; Gonzalez, C.; Martin, R. L.; Fox, D. J.; Defrees, D. J.; Baker, J.; Stewart, J. J. P.; Pople, J. A. *Gaussian 92/DFT*; Gaussian, Inc.: Pittsburgh, PA, 1992.
(17) Anderson, K.; Blomberg, M. R. A.; Fulscher, M. P.; Karlstrom, G.; Kello, V.; Lindh, R.; Malmqvist, P.-A.; Noga, J.; Olsen, J.; Roos, B. O.; Sadlej, A. J.; Siegbahn, P. E. M.; Urban, M.; Widmark, P.-O. *Molcas, Version 3*; University of Lund: Lund, Sweden.
(18) Almlof, J.; Taylor, P. R. *J. Chem. Phys.* **1987**, *86*, 4070.
(19) Hehre, W. J.; Ditchfield, R.; Pople, J. A. *J. Chem. Phys.* **1972**, *56*, 2257. Hariharan, P. C.; Pople, J. A. *Theor. Chim. Acta* **1973**, *28*, 213.
(20) Clark, T.; Chandrasekar, J.; Spitznagel, G. W.; Schleyer, P. V. *J. Comp. Chem.* **1983**, *4*, 294.
(21) Binkley, J. S.; Hehre, W. J.; Pople, J. A. *J. Am. Chem. Soc.* **1980**, *102*, 939.

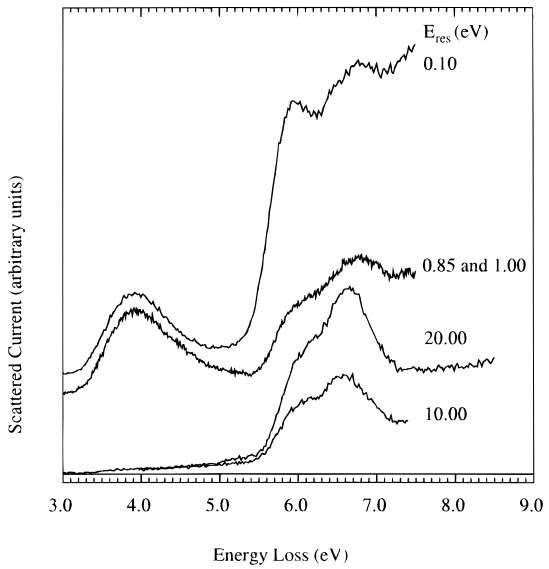

Figure 1. Electron energy-loss spectra of **1** obtained with residual energy values 0.10, 0.85/1.00, 10.0, and 20.0 eV. The 0.85/1.00 eV results are obtained by averaging the $E_{res} = 0.85$ and 1.00 eV spectra. The $E_{res} = 0.10$ and 0.85/1.0 spectra have been offset for clarity.

calculations on the higher-lying excited states. To circumvent this difficulty, a state-averaging procedure was adopted. For each symmetry, six states were included in the state-averaged CASSCF wave function, with each state being given equal weight. It was expected that this would give rise in both the singlet and triplet manifolds to the four $\pi \rightarrow \pi^*$ and 18 Rydberg states derived from $\pi \rightarrow$ 3s, $\pi \rightarrow$ 3p, and $\pi \rightarrow$ 3d excitations. However, in the triplet manifold, the two higher energy $\pi \rightarrow \pi^*$ states were "missed" by this procedure, and in their place $\pi \rightarrow \sigma^*$ states were obtained. An alternative strategy was therefore adopted to obtain energies for the higher lying $\pi \rightarrow \pi^*$ triplet states, namely, CASPT2 calculations were also carried out using an active space containing only the valence π and π^* orbitals with only two roots included in the state averaging.

To estimate the magnitude of the electronic couplings in the absence of through-bond interactions, calculations were also carried out on the excited states of a model ethylene dimer, with the two ethylene molecules separated and oriented as in **1**. The active spaces used for these calculations were the same as those employed for the full molecule.

3. Results

(1) Experimental Results. The electron energy-loss spectra were obtained with residual energies of 0.10, 0.85, 1.00, 10.0, and 20.0 eV. The spectrum obtained with the residual energy of 0.10 eV should be dominated by the structure due to the triplet states, and those obtained with residual energies of 10.0 and 20.0 eV should be dominated by the structure due to dipole-allowed singlet states. Dipole-forbidden singlet states are expected to appear most prominently in the $E_{res} = 0.85$ and 1.0 spectra. Figure 1 reports the $E_{res} = 0.10$, 0.85/1.0, 10.0, 20.0 eV, energy-loss spectra. The spectrum denoted 0.85/1.0 is the average of the $E_{res} = 0.85$ and 1.0 eV spectra.

The $E_{res} = 0.10$ eV spectrum displays peaks near 3.9, 5.9, and 6.7 eV. In addition, there is a weak shoulder near 6.5 eV. Based on the theoretical results, discussed below, we attribute the first peak to both the 1^3A_2 and 1^3B_1 $\pi \rightarrow \pi^*$ states, and the structure between 6.5 and 7.0 eV to the upper pair of triplet $\pi \rightarrow \pi^*$ states as well as to several Rydberg states. The pronounced peak near 5.9 eV is likely due to a core-excited anion state (see discussion at the end of this section). There may also be some contribution from the triplet $\pi_- \rightarrow$ 3s as well as the 1^1A_2 state at this energy.

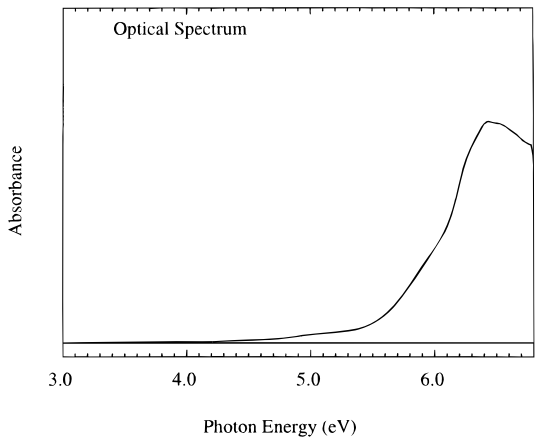

Figure 2. Optical absorption spectrum of **1** in acetonitrile solution.

The $E_{res} = 20.0$ eV spectrum displays a pronounced peak at 6.65 eV, with a shoulder near 6.2 eV. The peak at 6.65 eV is almost certainly due to the dipole-allowed ($1^1A_1 \rightarrow 1^1B_1$) $\pi \rightarrow \pi^*$ transition, whereas the shoulder near 6.2 eV is likely due to the dipole-forbidden ($1^1A_1 \rightarrow 1^1A_2$) $\pi \rightarrow \pi^*$ transition. The appearance of a dipole-forbidden transition in the $E_{res} = 20.0$ eV spectrum could be due to vibronic coupling with nearby dipole-allowed states. The low-energy shoulder (near 6.2 eV in the $E_{res} = 20$ eV spectrum) shifts downward about 0.2 eV and increases slightly in intensity in the $E_{res} = 10$ eV spectrum, consistent with there being more than one state near 6.0 eV. Again, the most likely candidate is one of the $\pi_- \rightarrow$ 3s or $\pi_- \rightarrow$ 3p singlet Rydberg states. The structure in the $E_{res} = 0.85$/1.0 eV spectrum closely resembles a superposition of that in the $E_{res} = 0.1$ and 10.0 eV spectra. In other words, both the singlet and triplet states are excited at residual energies near 1 eV.

The optical absorption spectrum measured in acetonitrile solution is shown in Figure 2. This spectrum displays a peak at 6.45 eV, with a weak shoulder near 6 eV. The spectrometer used for these measurements is limited to wavelengths greater than about 185 nm (6.7 eV), causing the cutoff in the measured spectrum. As in the gas-phase spectrum, the main peak is attributed to the dipole-allowed ($1^1A_1 \rightarrow 1^1B_1$) $\pi \rightarrow \pi^*$ transition and the shoulder near 6 eV to the dipole-forbidden ($1^1A_1 \rightarrow 1^1A_2$) $\pi \rightarrow \pi^*$ transition, the appearance of which could be due either to perturbations induced by the solvent or to vibronic coupling. Both the absorption spectrum in acetonitrile and the electron energy-loss spectra display a very weak diffuse feature near 5.2 eV. This is believed to be due to an impurity.

The excitation function for the lower pair of triplet states, obtained for a fixed energy loss of 3.9 eV, is reported in Figure 3. The peaks near 5.1 and at 6.45 eV in this excitation function are expected to arise from core-excited anion states which, upon electron detachment, decay into the 1^3B_1 and 1^3A_2 states. The lower energy core-excited anion state is expected to have the electronic configuration $\pi_+^2\pi_-\pi_+^{*2}(^2B_2)$, and the higher lying core-excited anion state is probably the 1^2A_1 state (involving the $\pi_+\pi_-^2\pi_+^{*2}$and $\pi_+^2\pi_-\pi_+^*\pi_-^*$ configurations, among others). The appearance of both of these core-excited states in the 3.9-eV energy-loss spectrum provides support for the interpretation that the 3.9-eV peak in the $E_{res} = 0.10$ eV spectrum is due to both the 1^3B_1 and 1^3A_2 $\pi \rightarrow \pi^*$ states. It is also likely that the core-excited anion state near 6.45 eV is partly responsible for the pronounced structure seen near 6.0 eV in the $E_{res} = 0.10$ eV spectrum.

(2) CASPT2 Calculations. The excitation energies for the $\pi \rightarrow \pi^*$ states calculated with the CASSCF, CASPT2, and CIS

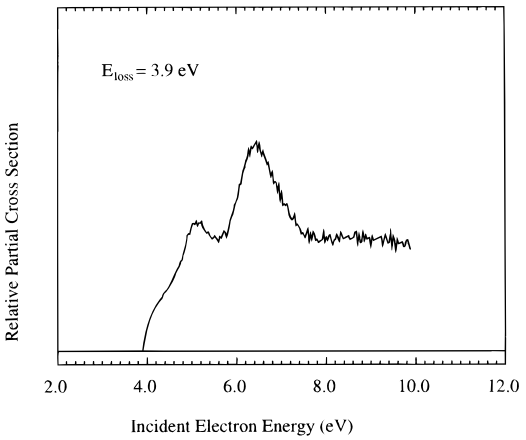

Figure 3. Excitation function of the two lowest energy $\pi \rightarrow \pi^*$ triplet states of **1** obtained for a fixed energy loss of 3.9 eV.

Table 1. Calculated Excitation Energies ΔE, $\langle x^2 \rangle$, $\langle y^2 \rangle$, and $\langle z^2 \rangle$ Expectation Values, and Oscillator Strengths of the $\pi \rightarrow \pi^*$ Excited States of **1**

	ΔE (eV)				$\langle x^2 \rangle$	$\langle y^2 \rangle$	$\langle z^2 \rangle$	osc.[c]
state	CASSCF	PT2	CIS[d]	ω[a]	(au)	(au)	(au)	strength
1^1A_1				0.68	52.3	57.9	55.0	
1^1A_2	8.63	5.84	6.35	0.62	63.0	64.0	58.0	0.00
1^1B_1	9.05	6.60	6.85	0.62	61.5	67.7	56.2	0.42
3^1B_1	11.20	7.30	*e*	0.60	56.5	65.6	54.3	*e*
5^1A_2	11.42	7.72	*e*	0.61	54.3	61.2	55.1	0.00
1^3A_2	4.17[f]	3.83[f]	3.51	0.63	54.8	59.2	55.7	0.00
1^3B_1	4.27[f]	3.93[f]	3.59	0.64	54.6	59.8	55.5	0.00
3^3B_1	11.38[f]	6.75[f]	8.21	0.55	54.7	59.5	55.5	0.00
3^3A_2	11.50[f]	6.82[f]	8.24	0.56	54.6	59.6	55.5	0.00

[a] ω gives the weight of the reference wave function in the CASPT2 calculations. [b] The $\langle x^2 \rangle$, $\langle y^2 \rangle$, and $\langle z^2 \rangle$ expectation values were calculated with the CASSCF wave functions. [c] The oscillator strengths (in au) were calculated using the CIS method. [d] All CIS excitation energies have been reduced by 0.6 eV. [e] The CIS calculations could not be converged for this state. [f] Results of calculations with two states averaged in the CASSCF wave function; the other CASSCF and CASPT2 results were obtained from calculations with six states averaged in the CASSCF wave function.

methods are reported in Table 1. This table also reports the weights of the reference wave functions in the CASPT2 wave functions and the $\langle x^2 \rangle$, $\langle y^2 \rangle$, and $\langle z^2 \rangle$ expectation values, calculated at the CIS level. The latter provide information about the valence and Rydberg character of the excited states. The weights of the dominant configurations in the CASSCF wave functions for the $\pi \rightarrow \pi^*$ states are given in Table 2.

The CASPT2 calculations predict the lowest energy $\pi \rightarrow \pi^*$ singlet state to be of A_2 symmetry with an excitation energy of 5.84 eV. The second and third $\pi \rightarrow \pi^*$ singlet states are predicted to be of B_1 symmetry and to lie at 6.60 and 7.30 eV, respectively. The second singlet $^1A_2$ $\pi \rightarrow \pi^*$ state is predicted to lie at 7.72 eV. The $\langle x^2 \rangle$, $\langle y^2 \rangle$, and $\langle z^2 \rangle$ expectation values for all four of these singlet states are relatively small, indicating that they are predominantly valence in character. These results are consistent with the interpretation that the 6.6-eV peak in the optical absorption and $E_{res} = 20$ eV energy-loss spectra is due to the ($1^1A_1 \rightarrow 1^1B_1$) $\pi \rightarrow \pi^*$ transition, and that the 6.0−6.2-eV feature seen in these spectra is due to the ($1^1A_1 \rightarrow 1^1A_2$) $\pi \rightarrow \pi^*$ transition.

The CASPT2 calculations, based on the CASSCF wave functions with only the two $\pi \rightarrow \pi^*$ states of either B_1 or A_2 symmetry state-averaged, give excitation energies of 3.83 and 3.93 eV for the lowest $^3A_2$ and $^3B_1$ states, respectively. The second set of $^3A_2$ and $^3B_1$ $\pi \rightarrow \pi^*$ states are predicted to lie about 2.9 eV higher in energy. In the absence of state averaging

Table 2. Weights of the Dominant Configurations in the CASSCF Wave Functions for the Ground State and $\pi \rightarrow \pi^*$ Excited States of **1**[a]

state	principal configurations	weights (%)
1^1A_1	$(\pi a_1)^2(\pi b_2)^2$	98
1^1A_2	$(\pi a_1)^2(\pi b_2)^1(\pi^* b_1)^1$	70
	$(\pi b_2)^2(\pi a_1)^1(\pi^* a_2)^1$	19
1^1B_1	$(\pi a_1)^2(\pi b_2)^1(\pi^* a_2)^1$	36
	$(\pi b_2)^2(\pi a_1)^1(\pi^* b_1)^1$	51
3^1B_1	$(\pi a_1)^2(\pi b_2)^1(\pi^* a_2)^1$	50
	$(\pi b_2)^2(\pi a_1)^1(\pi^* b_1)^1$	41
5^1A_2	$(\pi b_2)^2(\pi a_1)^1(\pi^* a_2)^1$	76
	$(\pi a_1)^2(\pi b_2)^1(\pi^* b_1)^1$	21
1^3A_2	$(\pi a_1)^2(\pi b_2)^1(\pi^* b_1)^1$	56
	$(\pi b_2)^2(\pi a_1)^1(\pi^* a_2)^1$	39
1^3B_1	$(\pi a_1)^2(\pi b_2)^1(\pi^* a_2)^1$	48
	$(\pi b_2)^2(\pi a_1)^1(\pi^* b_1)^1$	47
3^3B_1	$(\pi a_1)^2(\pi b_2)^1(\pi^* a_2)^1$	49
	$(\pi b_2)^2(\pi a_1)^1(\pi^* b_1)^1$	51
3^3A_2	$(\pi a_1)^2(\pi b_2)^1(\pi^* b_1)^1$	39
	$(\pi b_2)^2(\pi a_1)^1(\pi^* a_2)^1$	61

[a] These results for the triplet states were obtained from the calculations with two roots state averaged.

the CASPT2 calculations give vertical excitation energies of 3.94 ($^3A_2$) and 4.07 eV ($^3B_1$) for the lower two triplet states. Based on these results, we attributed the peak near 4 eV in the $E_{res} = 0.10$ eV energy-loss spectrum to the 1^3A_2 and 1^3B_1 states. The upper two $\pi \rightarrow \pi^*$ triplet states, along with a subset of the $\pi \rightarrow$ 3p Rydberg states, are probably responsible for the 6.7-eV peak seen in the $E_{res} = 0.10$ eV energy-loss spectrum. The CASPT2 calculations, based on the CASSCF wave function with six roots averaged, located the lowest $\pi \rightarrow \sigma^*$ triplet states at 8.63 ($^3A_2$) and 8.69 eV ($^3B_1$).

From Table 2 it is seen that the CASSCF wave functions for the lowest $^1A_2$ $\pi \rightarrow \pi^*$ state has much more weight from the $\pi_- \rightarrow \pi_+^*$ than from the $\pi_+ \rightarrow \pi_-^*$ configuration, whereas for the lowest $^1B_1$ $\pi \rightarrow \pi^*$ state and for the two low-lying $\pi \rightarrow \pi^*$ triplet states the two possible valence $\pi \rightarrow \pi^*$ configurations enter with roughly equal weight. This implies that there is appreciable charge-transfer character in the 1^1A_2 state, but that the other three $\pi \rightarrow \pi^*$ states in question have relatively little charge-transfer character. As a result a two-level model is more appropriate for describing triplet than singlet excitation transfer in the π^* manifold of **1**.

The theoretical results for the singlet and triplet Rydberg states are summarized in Tables 3 and 4, respectively. The states are numbered (e.g., 1^1B_1, 2^1B_1, etc.) in accordance with the energy orderings predicted by the CASPT2 calculations. For the low-lying Rydberg states, the energies of the singlet and triplet components are quite close, generally within 0.1 eV, as predicted in the CASPT2 calculations. The $\pi_- \rightarrow$ 3s Rydberg states are predicted to lie near 5.7 eV, followed by the $\pi_- \rightarrow$ 3p Rydberg states between 6.0 and 6.3 eV, and the $\pi_- \rightarrow$ 3d Rydberg states between 6.6 and 6.8 eV. From these results it is apparent that even the two lowest $\pi \rightarrow \pi^*$ singlet states are overlapped by a large number of Rydberg states. Although the spectra do not display sharp structure typical of Rydberg states, it is likely that the peark near 5.9 eV in the $E_{res} = 0.1$ eV spectrum and the shoulder near 6.2 eV in the 10 and 20 eV residual energy spectra derives in part from $\pi \rightarrow$ 3s and, perhaps also, $\pi \rightarrow$ 3p transitions. Similarly, one or more of the triplet $\pi_- \rightarrow$ 3d states could contribute to the peark near 6.8 eV in the $E_{res} = 0.1$ eV spectrum.

The $\pi_+ \rightarrow$ 3s states are predicted to lie near 7.0 eV, followed by the $\pi_+ \rightarrow$ 3p states near 7.3 eV, and spread by less than 0.1 eV, and by five closely spaced $\pi_+ \rightarrow$ 3d states starting at 7.7 eV. The CASPT2 calculations prediction that the $^1A_2$ $\pi_+ \rightarrow$

Table 3. Calculated Excitation Energies, $\langle x^2\rangle$, $\langle y^2\rangle$, and $\langle z^2\rangle$ Expectation Values, and Oscillator Strengths of the Singlet Rydberg States of **1**

state	ΔE (eV) CASSCF	PT2	CIS[d]	$\langle x^2\rangle$ (au)	$\langle y^2\rangle$ (au)	$\langle z^2\rangle$ (au)	ω^b	osc[c] strength
1^1A_1				52.3	57.9	55.0	0.68	
1^1B_2 ($b_2 \rightarrow 3s$)	6.02	5.75	5.72	77.3	88.0	86.5	0.67	0.025
2^1A_1 ($b_2 \rightarrow 3p$)	6.20	6.06	5.89	76.2	120.6	81.0	0.66	0.019
2^1B_2 ($b_2 \rightarrow 3p$)	6.48	6.25	6.33	77.1	69.5	124.7	0.67	0.023
2^1A_2 ($b_2 \rightarrow 3p$)	6.65	6.27	6.22	129.8	65.5	78.1	0.66	
3^1B_2 ($b_2 \rightarrow 3d$)	6.78	6.58	6.58	104.0	108.1	90.1	0.67	0.033
2^1B_1 ($b_2 \rightarrow 3d$)	6.96	6.67	6.53	122.7	102.9	74.4	0.66	0.030
3^1A_1 ($b_2 \rightarrow 3d$)	6.85	6.70	6.64	73.7	103.6	125.6	0.67	0.002
4^1B_2 ($b_2 \rightarrow 3d$)	6.95	6.77	6.82	113.3	60.2	133.3	0.65	0.001
3^1A_2 ($b_2 \rightarrow 3d$)	7.16	6.81	6.84	122.9	61.1	123.4	0.62	
4^1A_1 ($a_1 \rightarrow 3s$)	7.45	7.01	7.21	97.1	61.2	96.8	0.66	0.006
5^1A_1 ($a_1 \rightarrow 3p$)	7.68	7.33	7.57	78.0	72.6	128.3	0.66	0.009
5^1B_2 ($a_1 \rightarrow 3p$)	7.95	7.37	7.58	76.2	130.7	80.0	0.65	0.001
4^1B_1 ($a_1 \rightarrow 3p$)	7.86	7.38	7.53	132.3	73.4	80.8	0.66	0.011
4^1A_2 ($a_1 \rightarrow 3d$)	8.18	7.47	7.69	118.8	104.6	72.7	0.65	
6^1A_1 ($a_1 \rightarrow 3d$)	8.09	7.70	7.70	77.2	150.7	82.2	0.65	0.040
7^1A_1 ($a_1 \rightarrow 3d$)	7.90	7.77	*e*	119.4	60.3	127.3	0.67	
6^1B_2 ($a_1 \rightarrow 3d$)	8.06	7.77	7.76	73.3	112.2	125.9	0.66	0.008
5^1B_1 ($a_1 \rightarrow 3d$)	8.16	7.82	*e*	123.4	60.7	121.0	0.66	

[a] The $\langle x^2\rangle$, $\langle y^2\rangle$, and $\langle z^2\rangle$ expectation values were calculated using the CASSCF wave functions. [b] Weights of the CASSCF reference functions in the first-order wave functions. [c] The oscillator strengths (in au) were calculated using the CIS method. [d] All CIS excitation energies have been reduced by 0.6 eV. [e] The CIS calculations could not be converged for this state.

3d state lies 0.3 eV below its triplet counterpart is probably the result of valence/Rydberg mixing. As expected, the splittings between the Rydberg states resulting from excitations from π_+ and π_- orbitals correspond approximately with the experimentally measured[2] difference between the first and second ionization potentials (ΔIP = 0.87 eV).

(3) CIS Calculations. Due to the neglect of dynamical correlation effects, the excitation energies calculated with the CIS method tend to be higher than those calculated with the CASPT2 method. In order to facilitate comparison between the CASPT2 and the CIS results, the CIS excitation energies have been reduced by 0.6 eV. With this correction, the excitation energies of the Rydberg states as calculated with the CIS procedure agree on average to within 0.2 eV of the CASPT2 values. With the 0.6-eV reduction, the CIS calculations predict the lowest $^3A_2$ and $^3B_1$ $\pi \rightarrow \pi^*$ states to be 0.4−0.5 eV below the results from the CASPT2 calculations, and place the lowest $^1A_2$ and $^1B_1$ $\pi \rightarrow \pi^*$ states 0.25−0.5 eV higher in energy than predicted in the CASPT2 calculations.

The two lowest $^1B_1$ states are close in energy, with the CIS calculations placing the $^1B_1$ state derived from the $\pi_+ \rightarrow$ 3d excitation 0.32 eV below the lowest $^1B_1$ $\pi \rightarrow \pi^*$ state, but the CASPT2 calculations reverse the order, placing the valence $\pi \rightarrow \pi^*$ state 0.07 eV lower in energy. The mixing between these two configurations is reltively weak as evidenced by the fact that the oscillator strength calculated for the valence state is nearly 120 times larger than that for the Rydberg state.

Table 4. Calculated Excitation Energies and $\langle x^2\rangle$, $\langle y^2\rangle$, and $\langle z^2\rangle$ Expectation Values of the Triplet Rydberg States of **1**

state	ΔE (eV) CASSCF	PT2	CIS[c]	$\langle x^2\rangle$ (au)	$\langle y^2\rangle$ (au)	$\langle z^2\rangle$ (au)	ω^b
1^1A_1				52.3	57.9	55.0	0.68
1^3B_2 ($b_2 \rightarrow 3s$)	6.00	5.72	5.64	75.6	90.0	85.8	0.67
1^3A_1 ($b_2 \rightarrow 3p$)	6.15	6.02	5.78	75.8	121.4	80.1	0.66
2^3B_2 ($b_2 \rightarrow 3p$)	6.46	6.24	6.24	75.6	72.4	122.8	0.67
2^3A_2 ($b_2 \rightarrow 3p$)	6.49	6.34	6.23	124.3	65.1	76.4	0.66
3^3B_2 ($b_2 \rightarrow 3d$)	6.75	6.55	6.53	102.9	102.5	92.5	0.66
2^3B_1 ($b_2 \rightarrow 3d$)	6.82	6.70	6.52	115.7	96.7	72.3	0.66
2^3A_1 ($b_2 \rightarrow 3d$)	6.82	6.67	6.54	73.1	101.8	124.7	0.66
4^3B_2 ($b_2 \rightarrow 3d$)	6.94	6.77	6.80	115.4	60.0	130.8	0.66
4^3A_2 ($b_2 \rightarrow 3d$)	7.06	6.92	6.79	123.3	60.1	122.5	0.66
3^3A_1 ($a_1 \rightarrow 3s$)	7.43	7.00	7.15	95.7	61.2	98.2	0.66
4^3A_1 ($a_1 \rightarrow 3p$)	7.68	7.31	7.51	78.7	73.0	126.6	0.66
4^3B_1 ($a_1 \rightarrow 3p$)	7.74	7.46	7.47	134.2	77.6	81.1	0.66
5^3B_2 ($a_1 \rightarrow 3p$)	7.96	7.36	7.50	75.8	130.3	80.0	0.65
5^3A_1 ($a_1 \rightarrow 3d$)	8.01	7.65	7.56	76.7	149.1	80.0	0.65
6^3B_2 ($a_1 \rightarrow 3d$)	8.06	7.76	7.70	73.1	111.7	125.0	0.66
6^3A_1 ($a_1 \rightarrow 3d$)	7.89	7.77	7.76	118.4	60.2	126.9	0.67
5^3A_2 ($a_1 \rightarrow 3d$)	8.01	7.77	7.56	122.9	100.4	73.7	0.66
5^3B_1 ($a_1 \rightarrow 3d$)	8.00	7.86	7.74	123.3	60.0	119.3	0.66

[a] The $\langle x^2\rangle$, $\langle y^2\rangle$, and $\langle z^2\rangle$ expectation values were calculated using the CASSCF wave functions. [b] Weights of the CASSCF reference functions in the first-order wave functions. [c] All CIS excitation energies were reduced by 0.6 eV.

Table 5. $(T_1,T_2)^a$ and $(S_1,S_2)^b$ Splittings (eV) in **1** and the Ethylene Dimer Model Calculated with the CASPT2 and CIS Methods

		CASPT2/ ANO′	CIS/ 6-31+G*+spd	CASPT2/ 3-21G	CIS/ 3-21G
(T_1,T_2)	**1**	0.13	0.089	0.14	0.089
	dimer	6×10^{-3}	7×10^{-3}	6×10^{-4}	4×10^{-4}
(S_1,S_2)	**1**	0.76	0.49	0.88	0.603
	dimer	0.038	0.263	0.133	0.224

[a] Splitting between the two lowest $\pi \rightarrow \pi^*$ triplet states. [b] Splitting between the two lowest $\pi \rightarrow \pi^*$ singlet states.

(4) Splittings between the Lowest $\pi \rightarrow \pi^*$ States. Table 5 summarizes the splittings between the two lowest $\pi \rightarrow \pi^*$ triplet states (designated T_1 and T_2) and between the two lowest singlet $\pi \rightarrow \pi^*$ states (designated S_1 and S_2) of **1** and of the dimer model. Results were obtained with both the CASPT2 and CIS methods, and using both the 3-21G and ANO' or 6-31+G*+spd basis sets. The CIS and CASPT2 calculations with the flexible basis sets give T_1,T_2 ($1^3A_2 < 1^3B_1$) splittings on the order of $6-7 \times 10^{-3}$ eV for the ethylene dimer model. These splittings are about an order of magnitude larger than those obtained with

the 3-21G basis set, indicating that it is essential to employ flexible basis sets for describing the weak through-space interaction in the triplet manifold. On the other hand, for **1** the CIS calculations with both the 3-21G and 6-31+G*+spd basis sets give a T_1,T_2 splitting of about 0.09 eV, and the CASPT2 calculations with these two basis sets give T_1,T_2 splittings between 0.13 and 0.14 eV. The much larger T_1,T_2 splitting in **1** than in the ethylene dimer is due to the dominance of through-bond coupling in the former. The TB coupling, unlike the "direct" TS coupling, is well described by the 3-21G basis set.

A rather different picture emerges in the singlet manifold. Relatively large (up to 0.26 eV) S_1,S_2 ($1^1A_2 < 1^1B_1$) splittings are calculated for the ethylene dimer model. The much larger splitting between the singlet states than between the triplet states of the dimer is due to the dipole−dipole coupling mechanism operative in the singlet manifold. The S_1,S_2 splitting for the dimer obtained from the CASPT2/ANO' calculations (0.04 eV) is appreciably smaller than that obtained from the CASPT2/3-21G calculations or from either set of CIS calculations. This may reflect the importance of dynamic correlation effects in the $\pi \rightarrow \pi^*$ singlet state of ethylene. For **1**, the CIS and CASPT2 calculations with the 3-21G basis set give S_1,S_2 splittings of 0.60 and 0.88 eV, respectively. Somewhat smaller S_1,S_2 splittings are obtained with the more flexible basis sets, with the CIS/6-31+G*+spd and CASPT2/ANO' values being 0.49 and 0.76 eV, respectively. We conclude from these results that both the through-bond and dipole−dipole coupling mechanisms are important for the S_1,S_2 splitting, with the former making the larger contribution. It also follows that the TB coupling is larger in the singlet than in the triplet manifold.

(5) Discussion and Conclusions. The present electron energy-loss measurements do not give a measurable splitting between the two lowest triplet $\pi \rightarrow \pi^*$ triplet states of **1**. This indicates that the splitting between the T_1 and T_2 states is less than 0.2 eV, consistent with the CASPT2/ANO' and CIS/6-31+G*+spd calculations both of which give splittings of only about 0.1 eV. For norbornadiene CASPT2 calculations give a T_1,T_2 splitting of about 0.4 eV.[14] Thus, based on the calculations, the T_1,T_2 splitting falls off by about a factor of 4 in going from norbornadiene to **1**.

The electron energy-loss measurements give a splitting of 0.45 eV between the two lowest singlet $\pi \rightarrow \pi^*$ states of **1**. However, due to the overlap of valence and Rydberg states, there is an uncertainty of ±0.1 eV in the splitting. The S_1,S_2 splittings calculated with the CASPT2/ANO' and CIS/6-31+G*+spd methods are 0.76 and 0.50 eV, respectively, again in fairly good agreement with experiment. From comparison of the theoretical results for **1** with those for a ethylene dimer model, it is established that nearly all of the T_1,T_2 splitting and about 60−80% of the S_1,S_2 splitting in **1** is due to the through-bond mechanism. Most of the remainder of the splitting between the S_1 and S_2 states is due to dipole−dipole coupling. The TB contribution to the S_1,S_2 splitting of **1** is about 4.5 times larger than that to the T_1,T_2 splitting. The reason for the greater through-bond coupling in the singlet manifold is not clear at present.

Inclusion of dynamical correlation effects, absent in the CIS procedure, leads to about a 50% increase in both the T_1,T_2 and S_1,S_2 splittings. However, this does not necessarily mean that the CIS method would be inadequate for describing the rate of decrease in the electronic couplings in the $\pi \rightarrow \pi^*$ states along a series of bichromophoric molecules with increasing bridge lengths. The reason for this is that the net electronic coupling can be described (approximately) as a product of terms, one describing the coupling of the chromophores to the bridge and the other describing the propagation of the interaction along the bridge, the latter of which determines the distance dependence of the electronic coupling.[4] It may be that most of the increases in the T_1,T_2 and S_1,S_2 splittings brought about by inclusion of dynamical correlation effects are actually due to an enhanced coupling of the chromophore to the bridge, rather than the propgation of the interaction along the bridge. This possibility will be addressed in a future study.

Acknowledgment. This research was carried out with support of grants from the National Science Foundation and the Australian Research Council. We thank Dr. Zhenhuan Chz for measuring the absorption spectrum of **1** in acetonitrile.

JA9534664